Conjugated Polymer Nanodots as Ultrastable Long-Term Trackers to Understand Mesenchymal Stem Cell Therapy in Skin Regeneration

Guorui Jin, Duo Mao, Pingqiang Cai, Rongrong Liu, Nikodem Tomczak, Jie Liu, Xiaodong Chen, Deling Kong, Dan Ding, Bin Liu,* and Kai Li**

Stem cell–based therapies hold great promise in providing desirable solutions for diseases that cannot be effectively cured by conventional therapies. To maximize the therapeutic potentials, advanced cell tracking probes are essential to understand the fate of transplanted stem cells without impairing their properties. Herein, conjugated polymer (CP) nanodots are introduced as noninvasive fluorescent trackers with high brightness and low cytotoxicity for tracking of mesenchymal stem cells (MSCs) to reveal their in vivo behaviors. As compared to the most widely used commercial quantum dot tracker, CP nanodots show significantly better long-term tracking ability without compromising the features of MSCs in terms of proliferation, migration, differentiation, and secretome. Fluorescence imaging of tissue sections from full-thickness skin wound–bearing mice transplanted with CP nanodot-labeled MSCs suggests that paracrine signaling of the MSCs residing in the regenerated dermis is the predominant contribution to promote skin regeneration, accompanied with a small fraction of endothelial differentiation. The promising results indicate that CP nanodots could be used as next generation of fluorescent trackers to reveal the currently ambiguous mechanisms in stem cell therapies through a facile and effective approach.

1. Introduction

Stem cell–based therapies have attracted great attention in regenerative medicine (e.g., bone regeneration, cardiac repair, lung diseases, and wound healing),[1] which take advantage of the remarkable features of multipotency and self-renewal of stem cells.[2] Mesenchymal stem cells (MSCs) as adult stem cells have superiority in regenerative medicine because of the ethical concerns using embryonic stem cells.[3] While there has been a rapid surge in clinical trials involving MSCs, few treatments have been translated to humans due to contradictory results.[4] One of the reasons for the conflicting results is the lack of effective long-term cell tracking approaches that are able to promote comprehensive understanding of the fate (e.g., survival, migration, differentiation, and engraftment) of transplanted MSCs without impairing their intrinsic properties.[5] For instance, MSCs were found to contribute to wound repair by transdifferentiation into multiple skin cell types (including keratinocytes), while bioactive factors released by MSCs were found to make major contributions in skin regeneration through regulating the local cellular responses to injury.[6] However, the exact behaviors of transplanted MSCs (e.g., engraftment and migration) during skin regeneration have not been comprehensively deciphered, due to the lack of a feasible and reliable long-term stem cell tracking system.[7] As such, there is an urgent need to develop trustworthy cell tracking strategies to facilitate precise evaluation of the mechanism of MSCs in therapeutic treatment, which is essential for successfully harnessing stem cells in future clinical applications.[8]

Among versatile imaging techniques (e.g., positron emission tomography, fluorescence imaging, and magnetic resonance

Dr. G. Jin, Dr. R. Liu, Dr. N. Tomczak, Prof. B. Liu, Dr. K. Li
Institute of Materials Research and Engineering
A*STAR, 3 Research Link
Singapore 117602, Singapore
E-mail: cheliub@nus.edu.sg; lik@imre.a-star.edu.sg
D. Mao, Prof. D. Kong, Prof. D. Ding
State Key Laboratory of Medicinal Chemical Biology
Key Laboratory of Bioactive Materials
Ministry of Education
College of Life Sciences
Nankai University
94 Weijin Road, Tianjin 300071, China
E-mail: dingd@nankai.edu.cn
P. Cai, Prof. X. Chen
School of Materials Science and Engineering
Nanyang Technological University
50 Nanyang Avenue, Singapore 639798, Singapore
Dr. N. Tomczak
Department of Chemistry
National University of Singapore
3 Science Drive 3, Singapore 117543, Singapore
Dr. J. Liu, Prof. B. Liu
Department of Chemical and Biomolecular Engineering
National University of Singapore
4 Engineering Drive 4, Singapore 117585, Singapore

DOI: 10.1002/adfm.201501081

imaging),[9] fluorescence imaging shows advantages in providing a maneuverable nonionizing platform to visualize complex biological processes in high sensitivity with cellular level resolution.[10] To realize long-term tracking of transplanted stem cells, the fluorescent probes should be nontoxic with bright and stable fluorescence (both biologically and photophysically). As compared to the indirect labeling approaches by introducing fluorescent proteins or luciferase into cells, direct labeling methods enjoy the merits in easy operation and high labeling efficiency, which also avoid the safety issues associated with the viral vectors for transfection in indirect approaches.[11] Currently, the commercial quantum dot (QD)-based cell labeling kits possess superiorities over fluorescent dyes in terms of prolonged intracellular retention, better photostability, and lower background fluorescence from tissues due to their larger Stokes shifts.[12] However, QDs suffer from potential degradation caused by reactive oxygen species,[13] further resulting in fluorescence decrease and release of toxic heavy metal ions.[14] As a consequence, advanced exogenous fluorescent trackers with both outstanding cell tracking ability and negligible side effect to therapeutic stem cells remain in high demand.[10a,15]

Recently, conjugated polymers (CPs), a class of fluorescent macromolecules with highly delocalized π-conjugated backbones,[16] have emerged as a new generation of organic fluorescent nanomaterials with good photostability, high brightness, large Stokes shift, and low cytotoxicity.[17] Considering the aforementioned properties, CP holds great promises in the development of new noninvasive cell trackers to answer the unaddressed critical questions about cell fate during cell-based therapy. Although it has been reported that CPs have good biocompatibility in a variety of bioimaging tasks, the impact of CP probes on the behaviors of stem cells in long-term imaging and tracking has not been fully understood. In this contribution, we report the application of CP nanodots in tracking MSCs to reveal the mechanism of transplanted cells in promoting wound healing using a mouse model with full-thickness skin wounds. In vitro studies suggested that the effective labeling efficiency of MSCs after incubation with CP nanodots could remain ≈99.5% after continuous culture for 10 d, and the internalization of nanodots did not compromise the properties of MSCs in terms of proliferation, migration, differentiation, and secretome. Upon transplantation of CP nanodot-labeled MSCs to the wound sites, they showed similar healing progress using the mice treated with nanodot-free MSCs as the control. Immunofluorescence staining of regenerated tissues after transplantation for 21 d suggested that the transplanted MSCs remained within the dermis of regenerated skins with clear visualization of single cell morphology, which provided us insight in understanding how the transplanted stem cells contributed to the skin regeneration.

2. Results and Discussion

2.1. Preparation and Characterization of Trans-Activator of the Transcription (Tat)-CP Nanodots

Poly(9,9-dihexylfluorene-*alt*-2,1,3-benzoxadiazole) (PFBD) was synthesized according to literature.[18] 1,2-Distearoyl-*sn*-glycero-3-phosphoethanolamine-*N*-[methoxy(polyethylene glycol)-2000] (DSPE-PEG_{2000}) and its derivative, 1,2-distearoyl-*sn*-glycero-3-phosphoethanolamine-*N*-[maleimide(polyethylene glycol)-2000] (DSPE-PEG_{2000}-Mal), were then used to encapsulate PFBD to yield CP nanodots with surface maleimide groups. The maleimide-decorated PFBD nanodots were further conjugated with cell-penetrating peptide (RKKRRQRRRC) derived from HIV-1 Tat protein to afford Tat-PFBD nanodots.[19] The zeta potential of nanodots in water suspension changed from –29.2 ± 1.5 to 0.28 ± 0.04 mV after reaction with Tat peptide, indicating the successful conjugation of the peptide on nanodot surface. The obtained spherical Tat-PFBD nanodots (**Figure 1**A) had an effective average hydrodynamic diameter of 37 ± 7 nm (Figure 1B) and showed an intense absorption peak at 474 nm and an emission maximum at 583 nm in water (Figure 1C). The quantum yield (η) of Tat-PFBD nanodots in water was 42 ± 1% measured using 4-(dicyanomethylene)-2-methyl-6-(*p*-dimethylaminostyryl)-4H-pyran in methanol as a standard (η = 43%).[20]

The characterization of single Tat-PFBD nanodot was obtained by analyzing 354 single particles upon excitation at 488 nm. As shown in Figure 1D, individual bright single nanodot could be clearly visualized in the wide-field fluorescence image. The arithmetic average number of the total photons emitted by each Tat-PFBD nanodot is ≈9.72×10^5 counts per 100 s (Figure 1E), indicating the high brightness of each individual Tat-PFBD nanodot,[21] which is of high importance in real-time single dot tracking. To evaluate the reliability of Tat-PFBD nanodots in long-term bioimaging applications, the fluorescence stability of nanodots in biological medium was further monitored using commercial QD-based cell tracker, Qtracker 585, as the benchmark. After incubation at 37 °C for 35 d in Dulbecco's modified Eagle's medium (DMEM) supplemented with 10% fetal bovine serum (FBS), the suspension of Tat-PFBD nanodots remained above 90% of its initial fluorescence intensity (Figure 1F). On the contrary, Qtracker 585 in DMEM suspension suffered a sharp decrease to 26% of its initial value in 24 h and the intensity further dropped to only ≈10% of the initial value after 9 d. Overall, the high quantum yield and brightness as well as excellent fluorescence stability in biological medium are of high importance to ensure the accuracy and reliability of Tat-PFBD nanodots in long-term in vivo stem cell tracking.

2.2. In Vitro Tracking of MSCs Using Tat-PFBD Nanodots

The performance of Tat-PFBD nanodots in tracking MSCs was further evaluated using commercial Qtracker 585 as a reference. The MSCs were incubated with 4×10^{-9} M Tat-PFBD nanodots or Qtracker 585 for 4 h at 37 °C, respectively, followed by subculturing in fresh DMEM medium. After designated time intervals, the cells were detached to record fluorescence profiles using flow cytometry (λ_{ex} = 488 nm, 575/25 nm bandpass filter). As shown in **Figure 2**A, the labeling rate of MSCs treated by Tat-PFBD nanodots was 99.9% at day 0 and the high labeling rate could be maintained up to 10 d (99.5%). After continuously culturing for 25 d, 41.7% of MSCs were still effectively labeled. Noteworthy is that the MSCs incubated with 4×10^{-9} M Tat-PFBD nanodots for 1 h showed high labeling efficiency (99.0%) while only 0.5% of the cells were efficiently labeled after incubation with 4×10^{-9} M nonfunctionalized PFBD nanodots for 1 h,

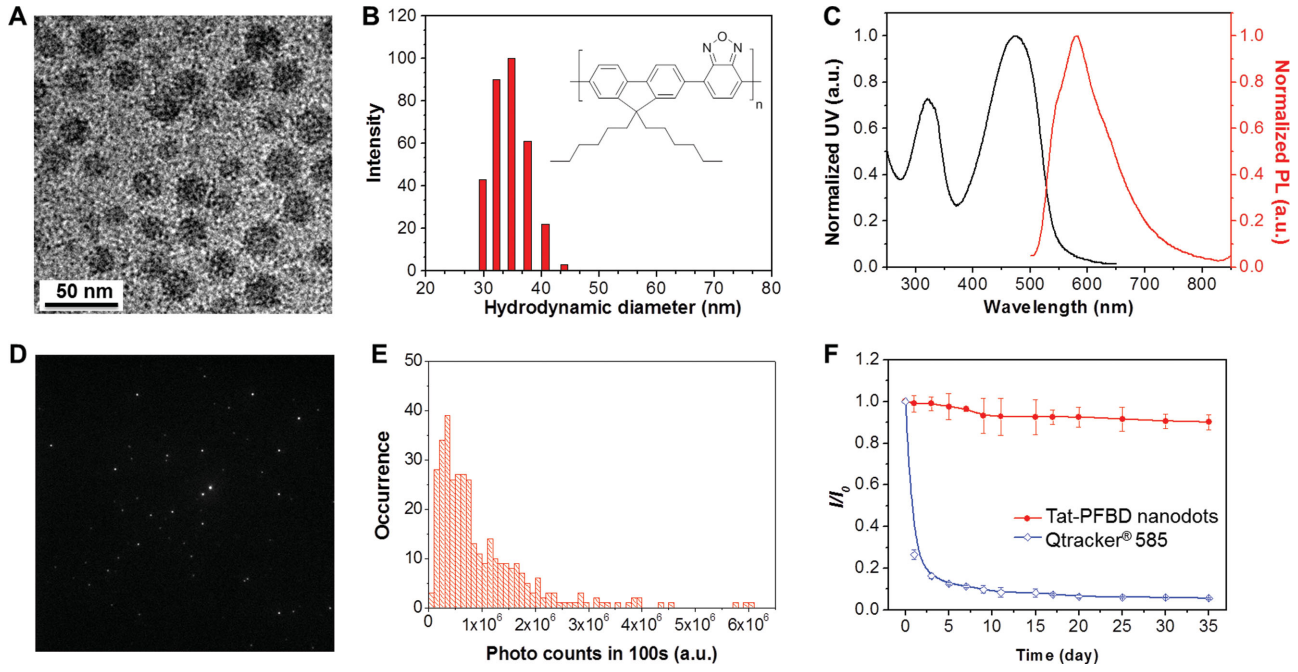

Figure 1. A) The morphology of nanodots under transmission electron microscopy. B) Particle size distribution of Tat-PFBD nanodots studied by dynamic light scattering. The inset shows chemical structure of PFBD. C) Absorption and emission spectra of Tat-PFBD nanodots in water suspension (λ_{ex} = 474 nm). D) Single particle fluorescence image of Tat-PFBD nanodots (image field: 80 μm × 80 μm). E) Histograms of the total number of photons collected during 100 s for each Tat-PFBD nanodot. F) Time courses of fluorescence intensity change of 4×10^{-9} M Tat-PFBD nanodots in DMEM supplemented with 10% FBS after continuous incubation at 37 °C. Data for Qtracker 585 are shown for comparison.

suggesting the importance of conjugation of Tat peptide to facilitate internalization of nanodots into living cells (Figure S1, Supporting Information). On the contrary, the labeling efficiency of Qtracker 585-treated cells was significantly decreased from 99.6% (day 0) to 50.0% at day 5 and only 14.1% of the cells were detectable after 10 d (Figure 2B). The fluorescence images indicated that the Tat-PFBD nanodots were homogeneously distributed in cell cytoplasm to give a clear visualization of the cell morphology, while only very weak fluorescence was detected in Qtracker 585-labeled cells after 5 d (Figure 2C). These results demonstrated the superior cell tracking ability of Tat-PFBD nanodots over Qtracker 585 in in vitro studies, due to the high labeling efficiency and stable fluorescence in biological environment.

2.3. Impact of Tat-PFBD Nanodots on MSC Behaviors

The ideal fluorescent cell trackers are expected to have minimal perturbation to the functions of transplanted stem cells that are generally sensitive and fragile to exterior stimuli. To address this issue, the behaviors (proliferation, migration, differentiation, and secretome) of MSCs treated with Tat-PFBD nanodots were investigated first, using nanodot-free MSCs as control. The in vitro proliferation of MSCs after labeling with 4×10^{-9} M Tat-FPBD was first evaluated by methylthiazolyl-diphenyl-tetrazolium bromide (MTT) assay. The cell metabolic activity results revealed that Tat-PFBD nanodot-labeled MSCs had similar cell number with the nanodot-free MSCs after further incubation in fresh medium for 3, 6, and 9 d (Figure S2A, Supporting Information). Additionally, the viability of MSCs remained above 90% after incubation with 4, 6, and 8×10^{-9} M Tat-PFBD nanodots for 72 h (Figure S2B, Supporting Information), confirming the low cytotoxicity of Tat-PFBD nanodots to MSCs. Furthermore, the motility of MSCs treated by Tat-PFBD nanodots was also investigated through an in vitro wound healing model. As demonstrated in Figure S2C (Supporting Information), the MSCs with or without nanodot labeling showed similar capability in migration, suggesting that Tat-PFBD nanodots had negligible effect on the cell migration ability.

Considering the capability of pluripotent differentiation is one of the key factors for MSCs in regenerative medicine, the differentiation of Tat-PFBD nanodot-labeled stem cells was quantitatively analyzed by reverse transcription polymerase chain reaction (RT-PCR). An early marker of epidermal differentiation,[22] keratin 10 (KRT10), and an intermediate marker of epidermal differentiation,[23] filaggrin (FLG), were chosen for analysis. Tat-PFBD nanodot-labeled MSCs and nanodot-free MSCs were separately cultured in an epidermal induction medium for 15 d,[24] followed by extraction of total RNA with the RNeasy Mini Kit, using KRT10 and FLG primers to analyze the relative endogenous mRNA. The Tat-PFBD nanodot-treated MSCs and nanodot-free MSCs showed no significant difference in expression levels of KRT10 and FLG mRNA (**Figure 3**A), confirming that the internalization of Tat-PFBD nanodots did not suppress MSC epidermal differentiation.

It has been well established that cellular mechanics and mechanotransduction could be able to dictate the fate of stem cells.[25] To investigate if cellular biomechanics altered as a result of nanodots internalization, high-resolution traction

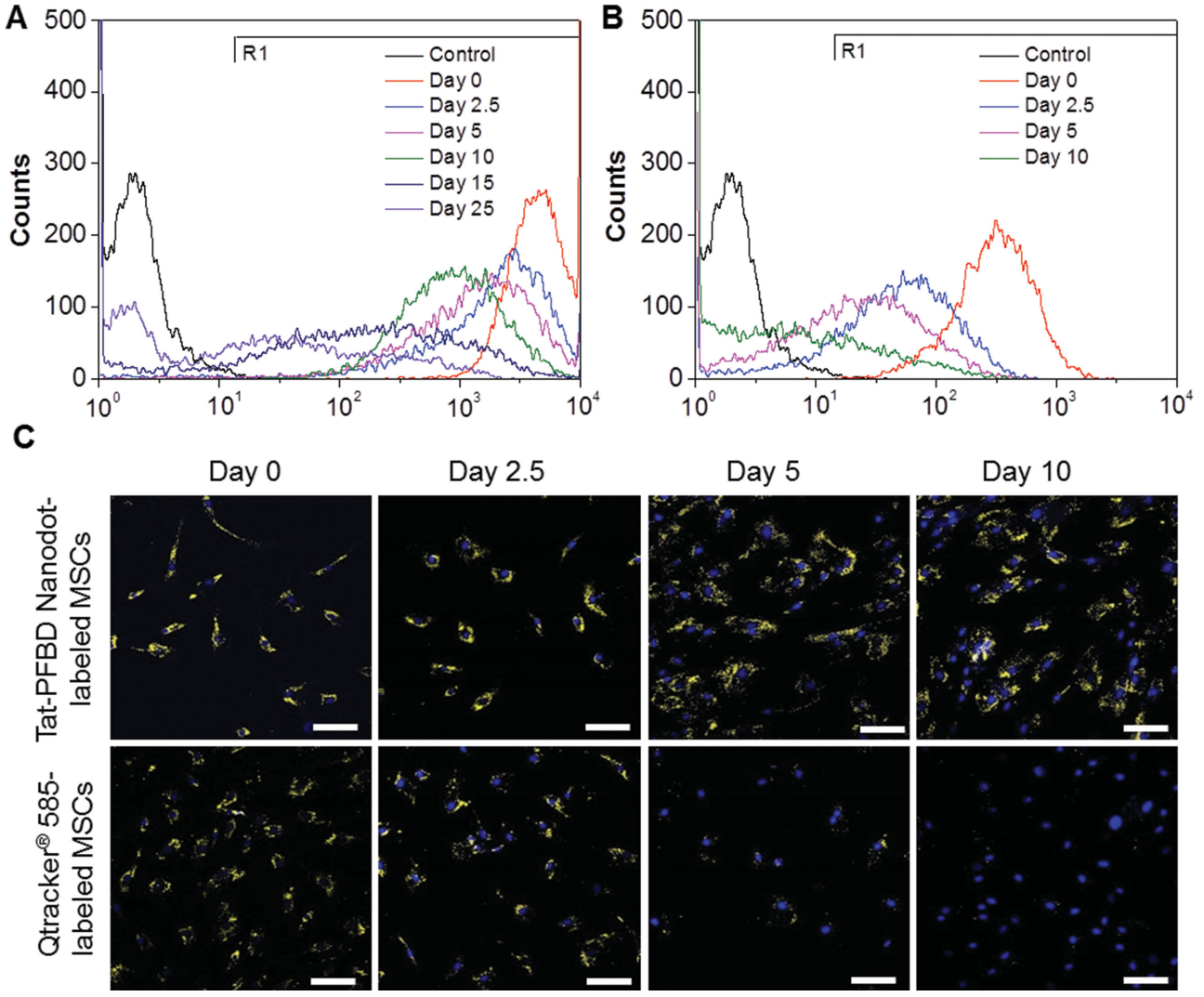

Figure 2. Flow cytometry histograms of MSCs after incubation with 4×10^{-9} M. A) Tat-PFBD nanodots and B) Qtracker 585 at 37 °C for 4 h and then subcultured for designated time intervals. The untreated MSCs were used as the control. C) The corresponding confocal images from both groups recorded under excitation at 488 nm with a 550–780 nm bandpass filter. The nuclei were stained with 4′,6-diamidino-2-phenylindole (DAPI) and the fluorescence was recorded upon excitation at 405 nm with a 430–470 nm bandpass filter. Scale bar = 100 μm.

force microscopy was used to determine the spatial distribution and traction stress in MSCs labeled with Tat-PFBD nanodots. MSCs with or without incubation of 4×10^{-9} M Tat-PFBD nanodots for 4 h were separately seeded on fibronectin-coated polyacrylamide (PAA) hydrogel homogeneously embedded with fluorescent microbeads and subsequently cultured in epidermal induction medium after MSCs attached and spread. At day 0 and day 15, cell traction forces (CTFs) were quantified through measuring the displacements of fluorescent beads before and after trypsinization of the attached MSCs. Statistical analysis of several individual cells (n = 10) suggested that Tat-PFBD nanodot-labeled and unlabeled MSC had no significant difference in average cell traction stress at the same time points (Figure 3B). The average traction stress of nanodot-labeled MSCs after differentiation (day 15) was ≈2.9 times as high as that before differentiation (day 0). In terms of traction stress mapping, both labeled and unlabeled MSCs showed an identical alteration of traction stress pattern before and after differentiation, namely, from polarized pattern to nonpolarized pattern (Figure 3C). Such similar spatial alteration of traction stress implies their transformation into epithelial phenotype.[26]

Paracrine signaling is another primary mechanism for the beneficial effects of MSCs on skin regeneration through reducing inflammation, promoting angiogenesis, and inducing cell migration and proliferation.[27] Thus, the secretome behaviors of Tat-PFBD nanodot-labeled and unlabeled MSCs were investigated by real-time PCR using nanodot-free dermal fibroblasts as reference. As shown in Figure 3D, the levels of paracrine cytokines, including interleukin 6 (IL-6), vascular endothelial growth factor A (VEGF-A), angiopoietin 1 (Ang-1), stromal cell–derived factor 1 (SDF-1), monocyte chemotactic protein 1 (MCP-1), basic fibroblast growth factor (bFGF), and transforming growth factor beta 1 (TGF-β1), did not show significant alteration from cells with or without Tat-PFBD nanodot

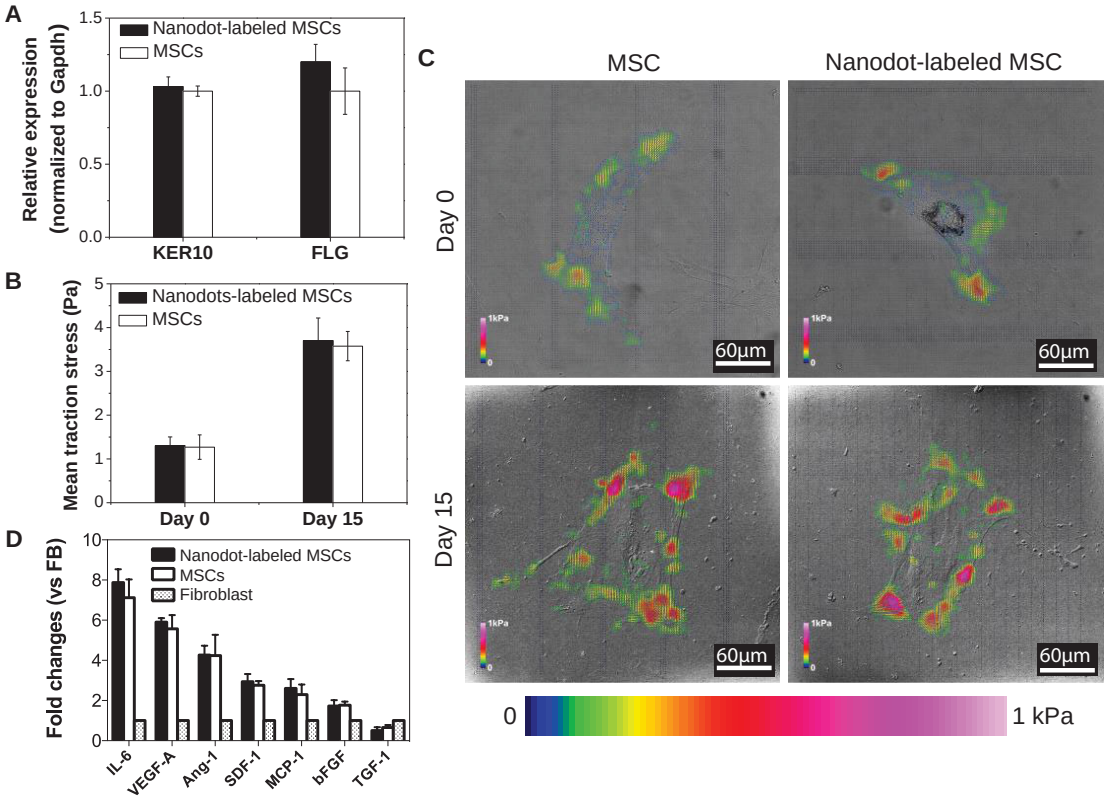

Figure 3. A) PCR results of KRT10 and FLG mRNA expression levels in Tat-PFBD nanodot-labeled (black) and unlabeled MSCs (white) that were cultured in epidermal induction medium after 15 d. B) The mean traction stress of Tat-PFBD nanodot-labeled (black) and unlabeled MSCs (white) on day 0 and day 15 (n = 10). C) Representative DIC images superimposed with color coded traction stress mapping of Tat-PFBD nanodot-labeled and unlabeled MSCs on day 0 and day 15. Scale bar = 60 μm. D) Secretome analyses for dermal fibroblasts (FB) and MSCs with and without Tat-PFBD nanodot labeling.

labeling, verifying that the nanodot did not obviously affect the secretome behavior of MSCs. Special attention should be paid to the cytokines (VEGF-A, Ang-1, SDF-1, and bFGF) that involve in angiogenesis. The expression levels of the four cytokines secreted from MSCs were significantly higher than that secreted from dermal fibroblasts, indicating that the paracrine signaling of MSCs is important in promoting skin regeneration. As a result, Tat-PFBD nanodots are suitable for tracking MSCs without compromising the cell behaviors of proliferation, migration, differentiation, and secretome, which will benefit the long-term in vivo cell tracking studies.

2.4. Tracking and Engraftment Evaluation of MSCs in Mice with Full-Thickness Wounds

The capability of Tat-PFBD nanodots for in vivo tracking and identifying the fate of transplanted MSCs was investigated using a full-thickness wound mouse model. A full-thickness excision wound was generated on the left dorsal skin of each eight-week mice, followed by transplantation of 1×10^6 MSCs labeled by Tat-PFBD nanodots using Matrigel as the substrate. A contralateral wound site on the same mice was also created on the right dorsal skin and transplanted with 1×10^6 nanodot-free MSCs. Luciferase and green fluorescent protein (GFP) double-expressing MSCs isolated from male FVB-luc-GFP transgenic mice were used in this study, which allowed in vivo monitoring of Tat-PFBD nanodot-labeled MSCs through both bioluminescence and fluorescence imaging to double confirm the reliability of Tat-PFBD nanodots in long-term cell tracking. Upon transplantation, intense fluorescence from the left wound site could be clearly distinguished at 1 h postwound infliction (PWI) (day 0) due to the bright emission from Tat-PFBD nanodots collected with a 560–900 nm filter (**Figure 4**A). Quantitative analyses of the fluorescent signals from left wound site revealed a continuous decrease in fluorescence intensity during the skin regeneration (Figure 4B). Meanwhile, the strong bioluminescence could be observed at both wound sites. The bioluminescence decay from both sites showed a homologous trend with fluorescence decay from the left wound site during the 21 d (Figure 4C). As luciferase labeling strategy is well-known for its accuracy in living cell tracking,[11] this result indicated the effectiveness and reliability of Tat-PFBD nanodots in long-term in vivo tracking of transplanted MSCs. Moreover, the bioluminescence intensity from transplanted MSCs with Tat-PFBD nanodot was similar to that from nanodot-free MSCs at each time point (Figure 4D), suggesting that the internalization of Tat-PFBD nanodots had minimized influence on the

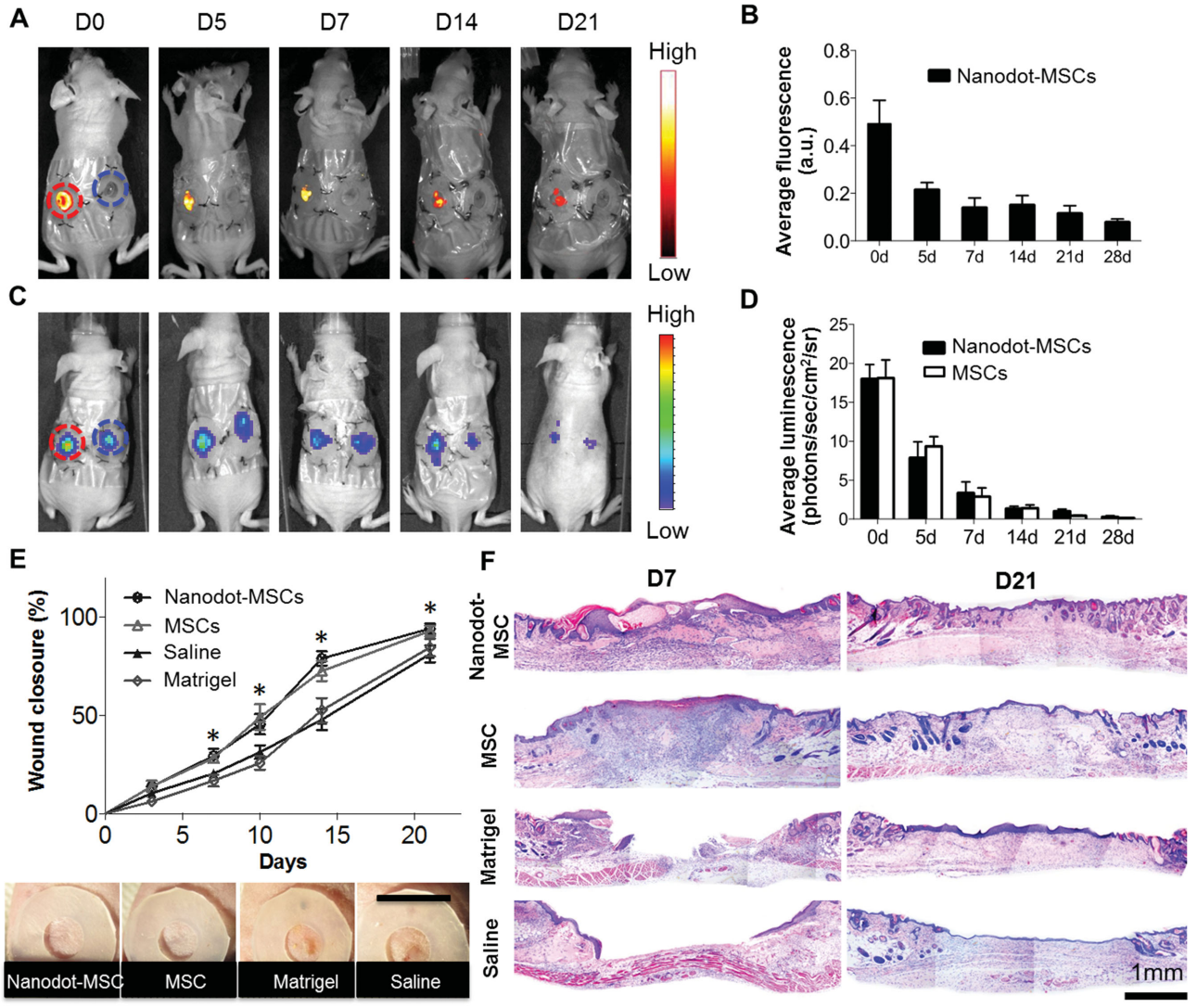

Figure 4. A) Representative in vivo fluorescence images of the wound sites on mouse transplanted with 1×10^6 GFP/luciferase double-expressing MSCs labeled with Tat-PFBD nanodots (left side wound) and that without nanodot labeling (right side wound) ($n = 8$ for each group). B) Time-dependent fluorescence intensity changes for the region of interest (ROI): the wound sites were identified by red and blue circles in (A). C) Corresponding in vivo luminescence images of the same mouse in (A). D) Time-dependent bioluminescence intensity changes for the ROI in (C). E) Percentages of epithelialized wound area in different groups from day 0 to 21. The digital photos show the wound sites of different groups at day 21. The scale bar is 1 cm. F) Histological analysis of skin tissues from the wound sites treated with Tat-PFBD nanodot-labeled MSCs, unlabeled MSCs, Matrigel and saline after 7 and 21 d.

bioluminescence imaging. The results further proved the priority of such organic nanodots in stem cell tracking as compared to commercial Qtrackers that were reported to greatly diminish the MSC function upon labeling, which failed to conclusively track cell location during in vivo bone regeneration study.[28]

The effect of Tat-PFBD labeling on regenerative function of MSCs during wound closure was studied using the mice with one full-thickness excision wound on the dorsal skin, followed by various treatments in four groups ($n = 8$ in each group). The sample group of mice was transplanted with Tat-PFBD nanodot-labeled MSCs on Matrigel in the wound sites, while the other three control groups of mice were separately treated with nanodot-free MSCs on Matrigel, saline, or Matrigel. The appearance of wound closure was recorded by digital camera and the wounds on mice transplanted with nanodot-labeled and unlabeled MSCs were both completely healed at day 21 with similar progress (Figure 4E and Figure S3, Supporting Information). Additionally, both of the two groups showed faster wound closure comparing to the ones treated with saline or Matrigel, indicating the importance of MSCs in promoting wound healing and the negligible impact of Tat-PFBD nanodots on stem cell properties in long-term in vivo tracking. Hematoxylin and eosin (H&E) staining results showed that the wounds in the MSC-treated groups were totally covered by the newly formed skin after 7 d, in contrast to the open wounds in the tissue sections collected from Matrigel and saline treated groups (Figure 4F). The newly formed epidermis and dermis

with hair follicles (bluish droplets) were found in the MSCs treated groups after 21 d, while the formation of epidermis was still undergoing without hair follicles in the Matrigel and saline treated groups.

We further investigated the application of Tat-PFBD nanodots in understanding the roles of MSCs during skin regeneration through studying the engraftment of transplanted nanodot-labeled MSCs in regenerated tissues. To evaluate the epidermal differentiation potential of transplanted MSCs and the progress of regeneration of epidermis, the skin tissue sections were collected from all groups after 5, 14, and 21 d for immunofluorescence staining. The results demonstrated that MSCs could accelerate wound healing process (Figures S4 and S5, Supporting Information and **Figure 5**A–C). After 21 d, the newly formed epidermis with similar expression of KRT10 and FLG was found in the skin sections collected from mice transplanted with MSCs (Figure 5A). However, the epidermis in skin sections collected from the saline treated mice was not completely formed in the epidermis layer (Figure 5B). More importantly, the labeled MSCs were found to distribute within the dermis (Figure 5C) and the enlarged image revealed that the internalized Tat-PFBD nanodots facilitated single cell identification with a bright yellow color after 21 d upon transplantation (Figure 5D). No KRT10 or FLG expression was found in Tat-PFBD nanodot-labeled cells (Figure 5C), indicating that the transplanted MSCs did not undergo epidermal differentiation during skin regeneration. The accuracy and reliability of Tat-PFBD nanodots during in vivo tracking of MCSs were then examined by taking advantages of the GFP expression in cells. Upon amplifying signal through GFP antibody/Alexa Fluor 633 staining, the apparent colocalization of signals from Tat-PFBD nanodots (yellow) and GFP antibody/Alexa Fluor 633 (red) in cytoplasm suggested the ability of Tat-PFBD nanodots for precise tracking of the transplanted cells in long-term regenerative treatments (Figure 5E). Quantitative analysis on day 21 based on ten confocal images from different fields of regenerated skin tissues for each mouse (n = 8) indicated that ≈86% of GFP-expressed MSCs were stained with bright Tat-PFBD nanodots.

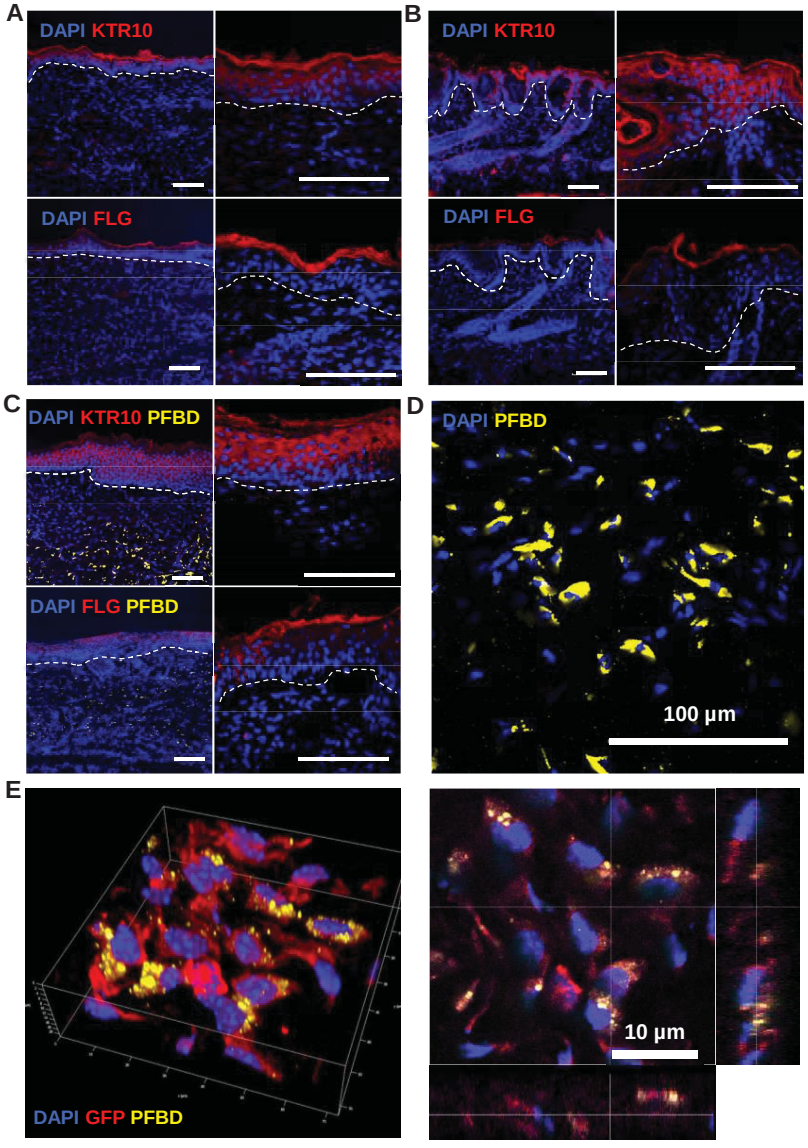

Figure 5. Confocal images of the regenerated skin tissue sections from mice treated with A) MSCs, B) saline, and C) Tat-PFBD nanodot-labeled MSCs after 21 d, respectively. The tissue sections were immunostained with KRT10 and FLG antibodies and revealed by Alexa Fluor 633. The generated epidermis was highlighted with dashed line. Scale bar is 100 μm for (A)–(D). D) The enlarged confocal imaging indicates the engraftment of Tat-PFBD nanodot-labeled MSCs in the regenerated skin. E) 3D confocal images of the regenerated skin tissue collected from mouse treated with Tat-PFBD nanodot-labeled MSCs. The red fluorescence is from GFP antibody/Alexa Fluor 633 and yellow signal is from Tat-PFBD nanodots in the transplanted MSCs. The nuclei were stained with DAPI.

To better understand the mechanisms of MSCs in promoting skin regeneration, the potential vascular differentiation of MSCs was studied through immunostaining of CD 31 as the indicator. The Tat-PFBD nanodots and CD 31 double positive cells were found in regenerated skin tissue section after 21 d (**Figure 6**A) and the nanodot-labeled MSCs were also found around the formed blood vessels (Figure S6, Supporting Information). The average intensities of fluorescent signals from CD31-stained tissue sections of different groups were also quantitatively analyzed by Image-J software (Figure 6B), suggesting that the mice treated with Tat-PFBD nanodot-labeled and unlabeled MSCs had higher densities of CD31-positive blood vessels in the regenerated skin tissues as compared to mice treated with Matrigel and saline. The expression of paracrine cytokines that regulate angiogenesis, VEGF, bFGF, and SDF-1, was further evaluated

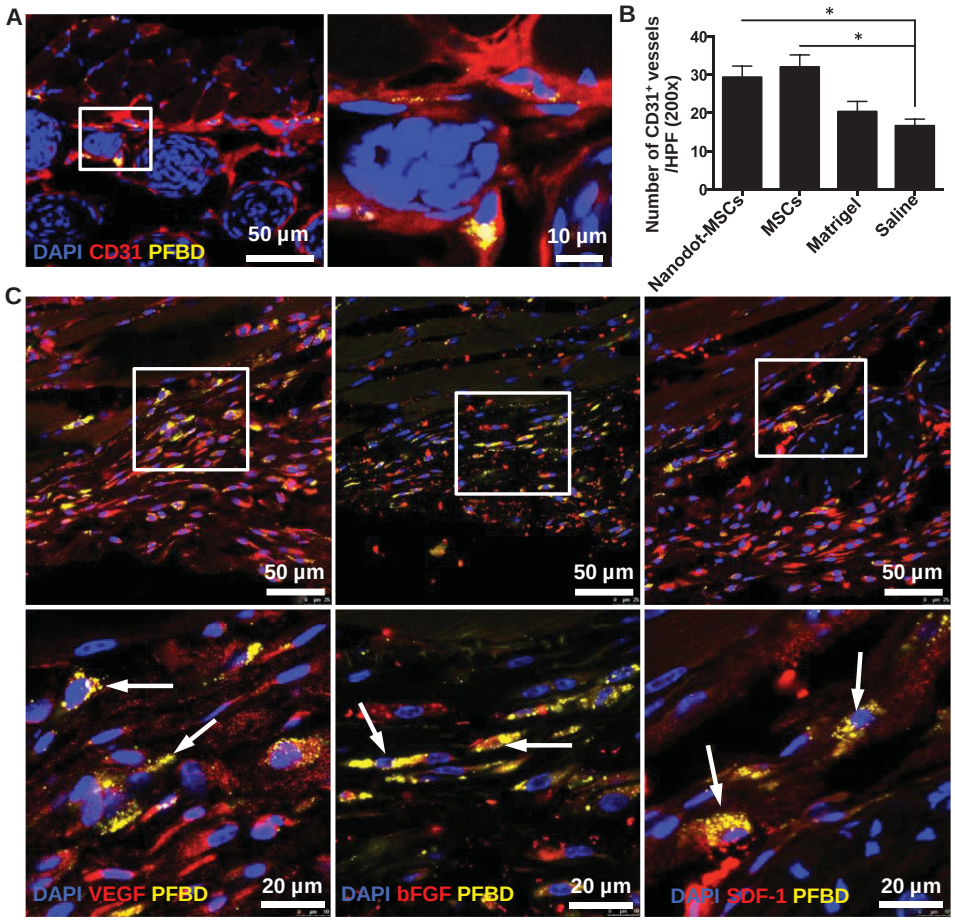

Figure 6. A) CD 31-stained images of the regenerated skin tissue from mouse treated with Tat-PFBD nanodot-labeled MSCs after 21 d. B) Quantitative analysis of neovascularization. C) Paracrine cytokines revealed by VEGF, bFGF, and SDF-1 antibody/Alexa Fluor 633 staining, respectively. The nuclei were stained with DAPI.

through immunostaining of the dermis of skin sections collected from mice transplanted with Tat-PFBD nanodot-labeled MSCs, using Alexa Fluor 633 as the fluorescent reporter. The colocalization of signals from Tat-PFBD nanodots (yellow) and targeted antibody (VEGF, bFGF, or SDF-1) (red) in cytoplasm confirmed that the nanodot-labeled MSCs secreted cytokines in vivo to promote skin regeneration (Figure 6C).

Taken together, these results demonstrated that despite the majority of the transplanted MSCs stayed within the dermis without differentiation, some transplanted MSCs could differentiate toward endothelial cells, instead of epidermal lineages, to promote neovascularization during skin regeneration. As the cells did not undergo direct differentiation into epidermal lineage in vivo, paracrine signaling of MSCs played the major role to promote skin regeneration in the mice with full-thickness wounds. These data proved that Tat-PFBD nanodots hold great promises as advanced fluorescent probes in tracking and visualizing the regenerative processes during stem cell therapies.

3. Conclusion

We demonstrated a noninvasive stem cell tracking strategy using biocompatible Tat-PFBD nanodots as the long-term fluorescent tracker, which revealed the mechanism of MSCs in promoting skin regeneration in a mouse model. Taking advantage of the unique features of high brightness, good fluorescence stability, and negligible interference with stem cell properties, the nanodots showed great potentials in both in vitro and in vivo tracking of MSCs with high effectiveness, accuracy, and reliability. Using GFP-expressed MSCs, the well overlap of signals from stained GFP and Tat-PFBD nanodots in cytoplasm of transplanted cells after 21 d confirmed the excellent performance of nanodots in long-term stem cell tracking. Moreover, the Tat-PFBD nanodots allowed detection of transplanted MSCs at single cell level in the regenerated tissues after immunofluorescence staining, identifying that they did not differentiate into epidermal lineage upon transplantation and the paracrine signaling was the primary contribution of MSCs in skin regeneration with a small fraction of vascular differentiation. Noteworthy is that this is the first report that CP-based nanomaterials were used as exogenous labeling probes for long-term stem cell tracking to investigate the roles of transplanted stem cells in regenerative medicine. To the best of our knowledge, this is the first time exogenous cell trackers could be used to clearly visualize the transplanted MSCs, which revealed that they did not undergo epidermal differentiation

because the cells were observed to remain in the regenerated dermis without migration to the epidermis. The facile labeling approach and reliable performance using Tat-CP nanodots as the fluorescent tracker is beneficial in providing valuable insights into the regenerative capacities of therapeutic stem cells, especially those cells with difficulties in transfection to express fluorescent proteins or luciferase. Further incorporation of other imaging reagents (e.g., radioactive and photoacoustic imaging reagents) will facilitate the development of multimodality trackers for translational research.

4. Experimental Section

Materials: PFBD was synthesized according to previous report. DSPE-PEG_{2000} and DSPE-PEG_{2000}-Mal were purchased from Avanti Polar Lipids, Inc. DMEM (low glucose), DMEM/nutrient mixture F12 (DMEM/F12), FBS, penicillin–streptomycin solution, 4′,6-diamidino-2-phenylindole, dihydrochloride (DAPI), Alexa Fluor 633 Phalloidin, and Qtracker 585 were all purchased from Life Technologies, Invitrogen, Singapore. Human bone marrow–derived MSCs were obtained from Lonza (Portsmouth, NH). Tetrahydrofuran (THF), dimethyl sulfoxide (DMSO), ascorbic acid, epidermal growth factor (EGF), 1,25-dihydroxyvitamin D_3 (VD_3), hydrocortisone, insulin, and 3,3,5-triiodo-L-thyronine sodium (T3) were all purchased from Sigma-Aldrich (Singapore). The RNeasy Mini Kit and the GAPDH, KRT10 and FLG primers were all purchased from Qiagen, Singapore. Cell penetrating peptide, HIV-1 Tat (50–57) with cysteine-modified terminus (RKKRRQRRRC), was customized by GenicBio, China.

Synthesis of Tat-PFBD Nanodots: A homogeneous THF solution containing PFBD, DSPE-PEG_{2000}, and DSPE-PEG_{2000}-Mal (1 mg each) was quickly injected into water, followed by continuous sonification using a probe sonicator at 12 W output (XL2000, Misonix Incorporated, NY). The suspension was then stirred vigorously at room temperature overnight to evaporate THF and yield PFBD nanodots in water (5 mL). The formed suspension was then filtered through a 0.2 μm syringe filter. The nanodots (2 mL) were further mixed with HIV1-Tat peptide (5×10^{-2} M) in the presence of DMSO (1×10^{-3} M). After overnight reaction at room temperature, the solution was dialyzed against MilliQ water for 2 d to eliminate the excess peptide. The PFBD nanodots were collected for further use.

Characterization: The UV–vis spectra were recorded on a Shimadzu UV-1700 spectrometer. The fluorescence spectra were measured using a fluorometer (LS-55, Perkin Elmer, USA). The average particle size and size distribution were determined by dynamic light scattering with a particle size analyzer (90 Plus, Brookhaven Instruments Co., USA) at a fixed angle of 90° at room temperature. The morphology of Tat-PFBD nanodots was studied by a high-resolution transmission electron microscope (TEM, JEM-2010, JEOL, Japan).

Single Nanoparticle Fluorescence Imaging: Fluorescence imaging of individual Tat-PFBD nanodot was performed with a wide-field microscope based on a Nikon ECLIPSE Ti-U inverted microscope frame. Light from a CW multiline Ar ion laser (λ_{ex} = 488 nm, Melles Griot, CA, USA) was fiber-coupled to a Nikon TIRF attachment and focused on the back aperture focal plane of a high NA objective (Nikon TIRF Apo 100×, NA = 1.49, oil immersion). Immersion oil was added between the high NA objective and the coverslip for refractive index matching. The luminescence was collected by the same objective and after passing through the dichroic mirror and the emission filter it was directed onto an iXonEM+897 EMCCD camera (512 pixels × 512 pixels, 150 nm per pixel resolution, Andor Technology, Northern Ireland) connected to the side port of the microscope. The camera was connected to a computer furbished with camera-dedicated software to control the imaging parameters, and for data acquisition. The samples were prepared by depositing a droplet of nanodot solution on a glass cover slide, followed by removing excess of liquid and drying under nitrogen. The reported intensity values are obtained after background subtraction. The background was obtained from a region on the glass slide where no nanodots were deposited.

In Vitro Cell Tracking: MSCs were cultured in six-well plates (Costar, IL, USA) to achieve 80% confluence. After medium removal and washing with 1× PBS buffer, 4×10^{-9} M Tat-PFBD nanodots or Qtracker 585 in DMEM medium was then added to the wells. After 4 h incubation at 37 °C, the cells were washed twice with 1× PBS buffer and detached by 1× trypsin and resuspended in culture medium. Upon dilution, the cells were subcultured in six-well plates containing cell culture coverslips (diameter 15 mm) for 2.5, 5, 10, 15, and 25 d, respectively. After designated time intervals, the coverslips within the six-well plates were removed and fixed by 4% paraformaldehyde for 15 min. The coverslips were then sealed with mounting medium and the fluorescence images were studied by a confocal microscope (Olympus Fluoview FV1000). The rest of MSCs within six-well plates were washed twice with 1× PBS buffer and detached by 1× trypsin for resuspension in 4% paraformaldehyde. The fluorescence profiles of cells were then recorded using flow cytometry by counting 10 000 events (λ_{ex} = 488 nm, 575/25 nm bandpass filter). In all flow cytometry tests, nanodot-free MSCs were used as the control.

Cytotoxicity of Tat-PFBD Nanodots: The metabolic activity of MSCs was evaluated by MTT assays to study the cytotoxicity of Tat-PFBD nanodots. MSCs were seeded in 96-well plates (Costar, IL, USA) at 2×10^4 cells mL^{-1}. After 24 h incubation, the medium was replaced by the Tat-PFBD nanodot suspension at concentrations of 4, 6, and 8×10^{-9} M, and the cells were then incubated for 48 and 72 h, respectively. After the designated time intervals, the wells were washed twice with 1× PBS buffer and 100 μL of freshly prepared MTT (0.5 mg mL^{-1}) solution in culture medium was added into each well. The MTT medium solution was carefully removed after 3 h incubation in the incubator at 37 °C. DMSO (100 μL) was then added into each well and the plate was gently shaken to dissolve all the precipitates formed. The absorbance of MTT at 570 nm was monitored by the microplate reader (Genios Tecan). Cell viability was expressed by the ratio of absorbance of the cells incubated with nanodot suspension to that of the cells incubated with culture medium only.

In Vitro Proliferation and Migration Study: MSCs were cultured in T-25 flasks (Costar, IL, USA) to achieve 80% confluence. After medium removal and washing with 1× PBS buffer, 4×10^{-9} M Tat-PFBD nanodots in DMEM medium was then added to the flask. After 4 h incubation at 37 °C, the cells were washed twice with 1× PBS buffer and detached by 1× trypsin and resuspended in culture medium. Upon dilution, the cells were seeded in 24-well plates at a density of 5×10^3 cells/well. MSCs without nanodots treatment were used as control. The cells were cultured for 3, 6, and 9 d. After designated time intervals, MTT assays were carried out to evaluate the metabolic activity of MSCs, compared to the untreated MSCs. MSC migration was evaluated using the monolayer scratch wound assay. The Tat-PFBD nanodot-labeled and unlabeled MSCs were seeded onto a round coverslips (15 mm diameter) located in a 24-well plate, and cultured until confluence. Next, the monolayer of MSCs was wounded with a 10 μL pipette tip, followed by washing with 1× PBS to eliminate the detached cells. Upon incubation for 12 and 24 h in fresh medium, the cells were fixed with 4% paraformaldehyde in PBS for 15 min and stained by DAPI/Alexa Fluor 633 phalloidin for fluorescence visualization of nuclei/actin filament. Images of the wounds were acquired by a confocal microscope (Olympus Fluoview FV1000).

Cell Traction Force Microscopy: The polyacrylamide gel films with embedded fluorescent microspheres were prepared according to literature and used for CTF microscopy study.[29] Briefly, a mixture of 2.5% acrylamide (Bio-Rad), 0.5% bis-acrylamide (Bio-Rad), tetramethylethylenediamine (TEMED, Bio-Rad), ammonium persulfate (APS, Bio-Rad), and fluorescent polystyrene microbeads (diameter 0.1 μm, Invitrogen) were added onto glass coverslips. The 25 μL droplet was covered by another coverslip, which was removed after polymerization. The gel substrate was ≈70 μm thick with a Young's elastic modulus of 10 kPa. Before cell seeding, the formed PAA gel

film was coated with 50 μg mL^{-1} of human plasma fibronectin (Sigma-Aldrich) overnight. To map the traction stress cell exerted on the substrate, the deformation field of the gel substrate was first determined by tracking fluorescent microbeads embedded right below the surface of the gel substrate. The displacement field of the microbeads was obtained by comparing images of the fluorescent microbeads before and after cell trypsinization. The deformation field of the gel substrate was then translated into traction stress field on the basis of Green's function. Briefly, the traction force at discrete point $\overline{f_1}$, located at the position (x_i, y_i) was calculated based on the following formulation: $\overline{u_t}(x,y) = \sum_{i=1}^{n} \vec{G}(x-x_i, y-y_i)\overline{f_1}$, where $\vec{G}$ denotes the Greens' tensor and u_t denotes the experimental displacements of fluorescent beads at position (x_i, y_i). The overall force of the cell (F) is an integral of the traction field magnitude over the area, $F = \int\int \sqrt{T_x^2(x,y) + T_y^2(x,y)}\, dx\, dy$, where $T(x,y) = [T_x(x,y) + T_y(x,y)]$ is the continuous field of traction vectors defined at any spatial position (x, y) within the cell. The average level of traction stress was calculated as overall traction forces divided by the area. The cell traction stress map was then integrated with the differential interference contrast (DIC) image of cells on gel substrate, and the corresponding traction stress was mapped in pseudocolor, which indicated regions of traction stresses (dark blue to light pink according to stresses from low to high).

In Vitro Differentiation Study: MSCs were induced to epidermal lineages to assess the effect of Tat-PFBD nanodots on stem cell differentiation. 4×10^{-9} M Tat-PFBD nanodots-labeled and unlabeled MSCs were seeded onto six-well plates at 1×10^4 cells mL^{-1}. After culturing overnight, the medium was replaced with epidermal induction medium comprising DMEM and Ham's F12 medium (3:1) including 10% FBS, 100 IU mL^{-1} penicillin, and 100 μg mL^{-1} streptomycin, supplemented with 0.4 μg mL^{-1} of hydrocortisone, 5 μg mL^{-1} of insulin, 1×10^{-9} M of T3, 10 ng mL^{-1} of EGF, 1×10^{-6} M of VD_3, and 50 μg mL^{-1} of L-ascorbic acid. All samples were incubated under standard culture conditions of 37 °C in a sterile humidified incubator with 5% CO_2 and the culture medium was changed every 4 d. After 15 d, quantitative evaluation of the targeted KRT10 and FLG mRNA was assessed by RT-PCR. RNA from each sample was extracted with the RNeasy Mini Kit (Qiagen, Singapore), according to the manufacturer's instruction. 500 ng of extracted RNA was used to synthesize cDNA by the SuperScript III kit (Invitrogen). Endogenous mRNA levels were measured by real-time PCR analysis based on SYBR Green detection with an ABI real-time PCR machine. The KRT10 and FLG primer pairs used were QuantiTect primer assays (Qiagen). Samples were analyzed three times and normalized to GAPDH.

Secretome Analyses of MSCs with and without Tat-PFBD Nanodot Labeling: Stem cells were incubated with Tat-PFBD nanodots and continued to culture for 5 d and then cells were analyzed by real-time PCR. Total RNA was extracted with TranZol Reagent (TransGen Biotechnology, Beijing, China). The PCR was performed in triplicate with the FastStart Universal SYBR Green Master (ROX; Roche, Mannheim, Germany) and ran on the iCycler iQ52.0 Standard Edition Optical System (Bio-Rad, Hercules, CA, USA). Primers used in PCR are listed in Table S1 (Supporting Information), which include VEGF-A, SDF-1, TGF-β1, bFGF, IL-6, MCP-1, and Ang-1. The results were analyzed against the housekeeping gene GAPDH.

Cell Culture: Luciferase+/GFP+ adipose-derived mesenchymal stem cells were isolated from the abdominal and inguinal adipose tissue of 8–12 weeks old male FVB-luc-GFP transgenic mice, which were subsequently cultured and expanded in 10 cm^2 plate in complete growth medium containing α-minimum essential medium supplemented with 10% FBS and 100 U mL^{-1} of penicillin–streptomycin at 37 °C in a humidified environment containing 5% CO_2. The culture medium was changed twice a week.

Wound Healing Model and MSCs Transplantation: All animal studies were performed in compliance with the guidelines set by Tianjin Committee of Use and Care of Laboratory Animals and the project protocols were approved by the Animal Ethics Committee of Nankai University. To create the mouse wound healing ischemic model, eight-week-old female BALB/c nude mice obtained from the Laboratory Animal Center of the Academy of Military Medical Sciences (Beijing, China) were randomly divided into four groups, and the excisional wound splinting model was generated. In brief, after anesthesia, two 6 mm full-thickness excisional skin wounds were created on each side of the midline. Wound received: 1×10^6 Tat-PFBD nanodot-labeled MSCs (Group I; $n = 8$), MSCs only (Group II; $n = 8$), Matrigel only (Group III; $n = 8$), and saline (Group IV; $n = 8$). For Tat-PFBD nanodot-labeled MSCs and nanodot-free MSCs transplantation, 5×10^5 MSCs in 50 μL of Matrigel (BD, Biosciences) were injected intradermally around the wound at four injection sites and 5×10^5 MSCs in 10 μL of Matrigel were applied onto the wound bed. For control groups, equal volumes of Matrigel and saline were implanted into excisional wounds in nude mice. A silicone splint was placed so that the wound was centered within the splint. An immediate-bonding adhesive (Krazy Glue, Columbus, OH, http://www.krazyglue.com) was used to fix the splint to the skin, followed by interrupted sutures to stabilize its position, and Tegaderm (3M, London, ON, Canada, http://www.3m.com) was placed over the wounds. The animals were housed individually.

In Vivo Cell Tracking: Fluorescence images were taken using the Maestro in vivo Imaging System (CRI Inc., Woburn, MA) after 0, 5, 7, 14, 21, and 28 d. The detection was set to capture images automatically at 10 nm increments from 560 to 900 nm with constant 1 s exposure. The obtained tagged image file format (TIFF) images were loaded into the vendor's software and analyzed. After fluorescence imaging, the mice were administrated with a solution of luciferase substrate (D-luciferin) and the bioluminescence intensity generated from oxidation of luciferin was recorded on a Xenogen IVIS Lumina II system for 5 min. The same mice were scanned for one month. Imaging signals were quantified in units of maximum photons per second per square centimeter per steridian. Bioluminescence imaging was performed by a researcher blinded to the study conditions.

Wound Closure Analysis: Digital photographs of wounds were taken at day 0, 3, 7, 14, and 28. Time to wound closure was defined as the time at which the wound bed was completely re-epithelialized and filled with new tissue. Wound area was measured by tracing the wound margin and calculated using an image analysis program (NIH Image). The researchers who measured the samples were blinded to group and treatment. The percentage of wound closure was calculated as follows: [(Area of original wound − Area of actual wound)/Area of original wound] × 100%. The inside edge of the splint exactly matched the edge of the wound, so that the splinted hole was used to represent the original wound size. Mice were sacrificed at 7, 14, and 28 d, at which times, skin samples including the wound and 4 mm of the surrounding skin were harvested using a 10 mm biopsy punch.

Histology and Immunohistochemistry: The skins from the wound site of mice were excised at 1, 2, and 3 weeks and were fixed in 4% paraformaldehyde for 24 h for histological staining. The tissue specimens were embedded in paraffin or optimal cutting temperature (OCT) compound, and cut into 6 μm thick sections, which were subjected to H&E staining. Images were observed under an inverted microscope (Nikon Eclipse TE2000-U Kanagawa, Japan) and analyzed by Nikon NIS Elements software. The regenerated skins from the wound site were also excised at 5, 14, and 21 d for and immunofluorescence staining. The fixed and frozen sections were stained with mouse antihuman KRT10 antibody (Thermo Fisher Scientific) and mouse antihuman FLG antibody (Thermo Fisher Scientific), respectively. Alexa Fluor 633 goat antimouse IgG (Life Technologies) was used as the secondary antibody to reveal KRT10 and FLG expression. The regenerated skin tissues from day 21 were further stained with rat anti-CD31 antibody (BD biosciences, USA), rabbit anti-PCNA antibody (Abcam, USA), rabbit anti-VEGF antibody (Abcam, USA), rabbit anti-GFP antibody (Abcam, USA), rabbit antibasic FGF antibody (Abcam, USA), and rabbit antibasic SDF-1 antibody (Abcam, USA). Alexa Fluor 633 goat antirabbit IgG (Life Technologies) and Alexa Fluor 633 goat antirat IgG (Life Technologies) were used as the secondary antibodies. The nuclei were stained with DAPI containing mounting solution (DAPI Fluoromount G, Southern Biotech, England). The sections without incubation with primary antibodies were used as negative controls. Slides were observed under confocal laser scanning microscopy (Leica TSC SP8, Germany).

Statistical Analysis: All quantitative results were obtained from at least three samples for analysis. Data were expressed as the mean ± standard error of the mean (SEM). A two-tailed paired Student's *t*-test was used to compare the differences. Difference with $p < 0.05$ was considered to be statistically significant.

Supporting Information

Supporting Information is available from the Wiley Online Library or from the author.

Acknowledgements

G.J. and D.M. contributed equally to this work. This work was supported by the National Basic Research Program of China (2011CB964903), the A*STAR Joint Council Office and Institute of Materials Research and Engineering of Singapore (13302FG056 and IMRE/13-8P1104), the Singapore National Research Foundation (R-279-000-444-281), the Singapore-MIT Alliance for Research and Technology (SMART) Innovation Grant (R279-000-378-592), and the National Natural Science Foundation of China (81301311 and 81220108015).

Received: March 18, 2015
Revised: May 2, 2015
Published online: May 29, 2015

[1] a) S. W. Lane, D. A. Williams, F. M. Watt, *Nat. Biotechnol.* **2014**, *32*, 795; b) P. S. Frenette, S. Pinho, D. Lucas, C. Scheiermann, *Annu. Rev. Immunol.* **2013**, *31*, 285; c) K. C. Wollert, H. Drexler, *Nat. Rev. Cardiol.* **2010**, *7*, 204; d) F. Barry, M. Murphy, *Nat. Rev. Rheumatol.* **2013**, *9*, 584; e) C. Blanpain, E. Fuchs, *Science* **2014**, *344*, 1242281; f) S. J. Forbes, N. Rosenthal, *Nat. Med.* **2014**, *20*, 857.

[2] a) L. da Silva Meirelles, A. M. Fontes, D. T. Covas, A. I. Caplan, *Cytokine Growth Factor Rev.* **2009**, *20*, 419; b) P. Bianco, X. Cao, P. S. Frenette, J. J. Mao, P. G. Robey, P. J. Simmons, C. Y. Wang, *Nat. Med.* **2013**, *19*, 35; c) A. I. Caplan, *J. Cell. Physiol.* **2007**, *213*, 341.

[3] C. Nombela-Arrieta, J. Ritz, L. E. Silberstein, *Nat. Rev. Mol. Cell Biol.* **2011**, *12*, 126.

[4] J. Ankrum, J. M. Karp, *Trends Mol. Med.* **2010**, *16*, 203.

[5] a) T. Kim, E. Momin, J. Choi, K. Yuan, H. Zaidi, J. Kim, M. Park, N. Lee, M. T. McMahon, A. Quinones-Hinojosa, J. W. M. Bulte, T. Hyeon, A. A. Gilad, *J. Am. Chem. Soc.* **2011**, *133*, 2955; b) K. Andreas, R. Georgieva, M. Ladwig, S. Mueller, M. Notter, M. Sittinger, J. Ringe, *Biomaterials* **2012**, *33*, 4515.

[6] a) C. Nie, D. Yang, J. Xu, Z. Si, X. Jin, J. Zhang, *Cell Transplant.* **2011**, *20*, 205; b) M. Sasaki, R. Abe, Y. Fujita, S. Ando, D. Inokuma, H. Shimizu, *J. Immunol.* **2008**, *180*, 2581; c) L. Chen, E. E. Tredget, P. Y. G. Wu, Y. Wu, *PLoS One* **2008**, *3*, e1886; d) S. C. Heo, E. S. Jeon, I. H. Lee, H. S. Kim, M. B. Kim, J. H. Kim, *J. Invest. Dermatol.* **2011**, *131*, 1559.

[7] a) Y. Wu, L. Chen, P. G. Scott, E. E. Tredget, *Stem Cells* **2007**, *25*, 2648; b) K. Ma, S. Liao, L. He, J. Lu, S. Ramakrishna, C. K. Chan, *Tissue Eng., Part A* **2011**, *17*, 1413.

[8] C. Xu, D. Miranda-Nieves, J. A. Ankrum, M. E. Matthiesen, J. A. Phillips, I. Roes, G. R. Wojtkiewicz, V. Juneja, J. R. Kultima, W. Zhao, P. K. Vemula, C. P. Lin, M. Nahrendorf, J. M. Karp, *Nano Lett.* **2012**, *12*, 4131.

[9] a) T. F. Massoud, R. Paulmurugan, S. S. Gambhir, *Nat. Med.* **2010**, *16*, 921; b) G. Hong, Y. Zou, A. L. Antaris, S. Diao, D. Wu, K. Cheng, X. Zhang, C. Chen, B. Liu, Y. He, J. Z. Wu, J. Yuan, B. Zhang, Z. Tao, C. Fukunaga, H. Dai, *Nat. Commun.* **2014**, *5*, 4206; c) E. T. Ahrens, J. W. M. Bulte, *Nat. Rev. Immunol.* **2013**, *13*, 755.

[10] a) K. Li, W. Qin, D. Ding, N. Tomczak, J. Geng, R. Liu, J. Liu, X. Zhang, H. Liu, B. Liu, B. Z. Tang, *Sci. Rep.* **2013**, *3*, 1150; b) T. J. Wu, Y. K. Tzeng, W. W. Chang, C. A. Cheng, Y. Kuo, C. H. Chien, H. C. Chang, J. Yu, *Nat. Nanotechnol.* **2013**, *8*, 682; c) M. L. James, S. S. Gambhir, *Physiol. Rev.* **2012**, *92*, 897.

[11] A. V. Naumova, M. Modo, A. Moore, C. E. Murry, J. A. Frank, *Nat. Biotechnol.* **2014**, *32*, 804.

[12] a) K. Pu, A. J. Shuhendler, J. Rao, *Angew. Chem. Int. Ed.* **2013**, *52*, 10325; b) K. Pu, A. J. Shuhendler, M. P. Valta, L. Cui, M. Saar, D. M. Peehl, J. Rao, *Adv. Healthcare Mater.* **2014**, *3*, 1292.

[13] a) Q. Pi, W. Zhang, G. Zhou, W. Liu, Y. Cao, *BMC Biotechnol.* **2010**, *10*, 36; b) A. B. Rosen, D. J. Kelly, A. J. T. Schuldt, J. Lu, I. A. Potapova, S. V. Doronin, K. J. Robichaud, R. B. Robinson, M. R. Rosen, P. R. Brink, G. R. Gaudette, I. S. Cohen, *Stem Cells* **2007**, *25*, 2128; c) K. T. Yong, W. C. Law, R. Hu, L. Ye, L. Liu, M. T. Swihart, P. N. Prasad, *Chem. Soc. Rev.* **2013**, *42*, 1236.

[14] Y. Su, M. Hu, C. Fan, Y. He, Q. Li, W. Li, L. h. Wang, P. Shen, Q. Huang, *Biomaterials* **2010**, *31*, 4829.

[15] K. Li, B. Liu, *Chem. Soc. Rev.* **2014**, *43*, 6570.

[16] a) K. Li, D. Ding, D. Huo, K.-Y. Pu, N. N. P. Thao, Y. Hu, Z. Li, B. Liu, *Adv. Funct. Mater.* **2012**, *22*, 3107; b) G. Feng, K. Li, J. Liu, D. Ding, B. Liu, *Small* **2014**, *10*, 1212.

[17] a) C. Wu, B. Bull, C. Szymanski, K. Christensen, J. McNeill, *ACS Nano* **2008**, *2*, 2415; b) K. Li, B. Liu, *J. Mater. Chem.* **2012**, *22*, 1257; c) C. Zhu, L. Liu, Q. Yang, F. Lv, S. Wang, *Chem. Rev.* **2012**, *112*, 3086; d) Z. Tian, J. Yu, C. Wu, C. Szymanski, J. McNeill, *Nanoscale* **2010**, *2*, 1999.

[18] Y. Li, J. Liu, B. Liu, N. Tomczak, *Nanoscale* **2012**, *4*, 5694.

[19] S. Piantavigna, G. A. McCubbin, S. Boehnke, B. Graham, L. Spiccia, L. L. Martin, *BBA Biomembr.* **2011**, *1808*, 1811.

[20] J. M. Drake, M. L. Lesiecki, D. M. Camaioni, *Chem. Phys. Lett.* **1985**, *113*, 530.

[21] D. Ding, D. Mao, K. Li, X. M. Wang, W. Qin, R. R. Liu, D. S. Chiam, N. Tomczak, Z. M. Yang, B. Z. Tang, D. L. Kong, B. Liu, *ACS Nano* **2014**, *8*, 12620.

[22] M. Mizoguchi, Y. Suga, B. Sanmano, S. Ikeda, H. Ogawa, *J. Dermatol. Sci.* **2004**, *35*, 199.

[23] N. Fusenig, *Effects of Mesenchymal Cells on Keratinocytes*, Cambridge University Press, London **1994**.

[24] G. Jin, M. P. Prabhakaran, S. Ramakrishna, *Acta Biomater.* **2011**, *7*, 3113.

[25] A. J. Engler, S. Sen, H. L. Sweeney, D. E. Discher, *Cell* **2006**, *126*, 677.

[26] E. Yim, M. Sheetz, *Stem Cell Res. Ther.* **2012**, *3*, 41.

[27] M. Z. Ratajczak, M. Kucia, T. Jadczyk, N. J. Greco, W. Wojakowski, M. Tendera, J. Ratajczak, *Leukemia* **2012**, *26*, 1166.

[28] K. M. Dupont, K. Sharma, H. Y. Stevens, J. D. Boerckel, A. J. García, R. E. Guldberg, *Proc. Natl. Acad. Sci. U.S.A.* **2010**, *107*, 3305.

[29] M. Dembo, Y. L. Wang, *Biophys. J.* **1999**, *76*, 2307.